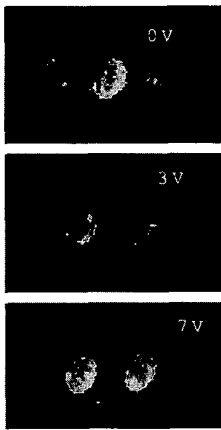
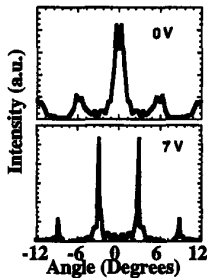


CFH4 Fig. 1 Schematic of the single-element phase-modulator grating device. Insets depict the response of the reflected beam with zero bias and positive bias.



CFH4 Fig. 2 Experimental response of the single-element phase-modulator grating at 0, 3 V, and 7 V.



CFH4 Fig. 3 Simulated response of the single-element phase-modulator grating at 0 V and 7 V including the effects of isotropic grating etching using wet chemical etchants.

The individual epitaxial layer structure consists of a vertical-cavity phase-flip Fabry-Perot modulator with a cavity containing AlGaAs/GaAs quantum wells surrounded by AlAs/AlGaAs quarter-wave mirror stacks. The specific wafer used for the array has modest performance (though better performance modulators have been produced). The on and off state reflectivity for the phase modulator is 40%, and the device switches

from 0° to 180° with 7V applied bias. The grating mesa itself is a 100 μm × 100 μm square vertical p-i-n diode. A physical grating with a period of 10 μm is formed (using 8-μm stripes, 2-μm spaces) by etching through portions of the mesa's p-type and intrinsic regions using a wet chemical etch. This permits a phase grating of 20-μm period. Figure 2 shows the far-field reflectivity from the grating at three voltages. Normal incidence laser light at 8310 Å was used in this case. As can be seen, at zero bias, the main reflectivity peak is at an angle of 0° while with 7 V bias, the light is scattered to the first-order diffraction peaks (at angles of 2.8°). The insets to Fig. 3 show the simulated response of the grating at the corresponding voltages accounting for the effects of the wet chemical etching. The device contains no moving parts so its speed is limited primarily by the reverse biased diode's RC constant. Geometry considerations thus prevail.

Beyond the two-state diffraction grating, we have investigated the variable pitch phase-diffraction grating, which is formed by making each of the individual device elements independently electrically addressable. Efficiency measurements and calculations will be presented. For example, the effects of sidewall-etching techniques critically determine the grating's efficiencies and are correlated to grating performance.

We believe such efficient electrically controllable gratings will have wide use for compact optical routing, interconnect, sensing, and imaging applications.

1. J. A. Trezza, J. S. Harris, Jr., *J. Appl. Phys.* 75, 4878 (1994).

CFH5 11:45 am

Single-chip photonic banyan network realized by arrays of beam-steering VCSELs and reflective Fresnel zone plates

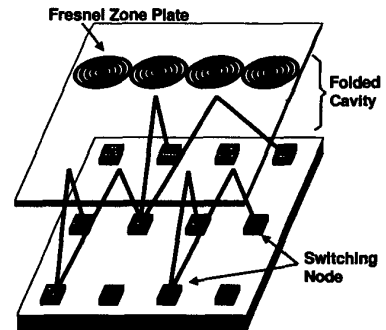
L. Fan, M. C. Wu, H. C. Lee,\* P. Grodzinski,\* *UCLA, Electrical Engineering Department, 66-147D, Engineering IV, Box 951594, Los Angeles, California 90095-1594*

Reconfigurable optical interconnection networks can significantly improve the performance of massively parallel processors and high-performance computer networks. Previously, we have demonstrated a single-chip 4 × 4 reconfigurable optical interconnection network by using arrays of beam-steering vertical-cavity surface-emitting lasers (VCSELs) with integrated photodetectors.<sup>1</sup> Different optical interconnections are established by space-division switching in free-space, i.e., by turning on VCSELs with different steering angles. The steering angle of VCSEL is precisely controlled by photolithographic and etching processes. This scheme requires only an external reflector. However, the interconnection density is limited by the divergence angle of the light emitted from VCSEL. In this paper, we report on the improved performance of the single-chip photonic Banyan network by replacing the planar mirror with an array of focusing mirrors.

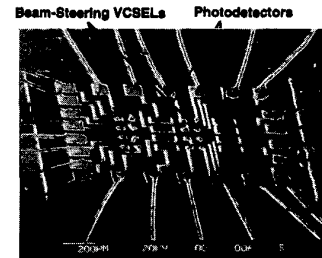
The schematic structure of the single-chip optical Banyan network combined with Fresnel zone plate is illustrated in Fig. 1. Each switching element consists of a photodetector and two beam-steering VCSELs. The beam-steering VCSEL is realized by integrating an optical beam router on the VCSEL.<sup>2</sup> The focusing mirror array serves two important functions: First, it bends the optical beams back to the photodetector of the switching node in the next stage so that all the active optoelectronic devices can be integrated on a single substrate. Second, the mirrors focus the steered light to the proper photodetectors to minimize optical crosstalk. The focusing mirror is realized by an array of reflective Fresnel zone plates.

Figure 2 shows the scanning electron micrograph (SEM) of the 4 × 4 photonic Banyan chip. The beam router is created by multiple-step etching on the surface of VCSEL. It is important that each step height is half-wavelength thick so that it will not perturb the fundamental mode operation or increase the threshold current. The routing angles of each VCSEL have been precisely controlled by photolithographic process. The photonic Banyan chip is packaged in a standard DIP IC package and capped with the external Fresnel zone plate array whose focal length is matched to the depth of the IC package. Alignment markers on the VCSELs and Fresnel zone plates allows precise lateral alignment.

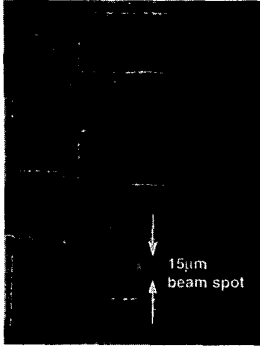
The beam spot projected on the photodetector has been measured with a



CFH5 Fig. 1 Schematic diagram of the 4 × 4 photonic Banyan network with reflective Fresnel zone plate array.



CFH5 Fig. 2 SEM micrograph of a packaged 4 × 4 photonic Banyan network.



CFH5 Fig. 3 Optical beam illuminated on the photodetectors when the reflective Fresnel zone plate is used. The beam spot is reduced to 15 μm.

CCD camera. With a planar mirror, the divergence angle of the three-step VCSEL with 6-μm-wide step is 2.8°. After traveling through the cavity and bouncing back from the external mirror, the spot size is increased to 220 μm. The interconnection density is therefore limited. Figure 3 shows the beam spot size obtained with the Fresnel zone plate array. The FWHM spot size has been reduced to 15 μm. With this approach, the areas of the photodetector can be reduced and the optical cross talk will also be improved. The cross talk between different adjacent channels is presented at the conference.

In conclusion, a single-chip photonic Banyan network has been demonstrated by using beam-steering VCSELs and reflective Fresnel zone plate array. The focusing mirror reduces the beam spot to 15 μm, and can greatly increase the optical interconnection density.

This project is supported by ARPA ULTRA through Army Research Laboratory under contract no. DAAL01-93-K-3533 and the Packard Foundation.

\*Motorola Inc. Phoenix Corporate Research Laboratories

1. L. Fan, M. C. Wu, H. C. Lee, P. Grodzinski, in *Proceedings of Massively Parallel Processing Using Optical Interconnections*, pp. 28-34 (1995).
2. L. Fan, M. C. Wu, H. C. Lee, P. Grodzinski, *Electron. Lett.* 31, 729-730 (1995).
3. K. Rastani, A. Marrakchi, S. F. Habiby, W. M. Hubbard, H. Gilchrist, R. E. Nahory, *Appl. Opt.* 30, 1347-54 (1991).

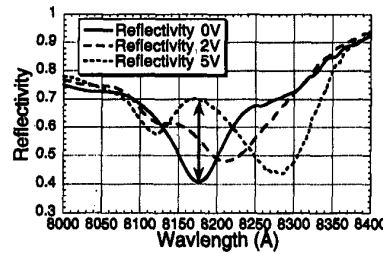
CFH6 12:00 m

**Zero-chirp asymmetric Fabry-Perot reflection electroabsorption modulator using coupled quantum well active region**

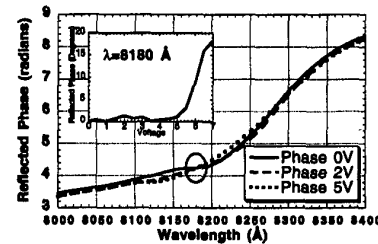
J. A. Trezza, J. S. Harris, Jr., 226 McCullough Bldg, Solid State Laboratories, Stanford University, Stanford, California 94305

While single quantum wells are capable of large absorption changes ( $\Delta\alpha$ ), their switching speed is limited by large re-

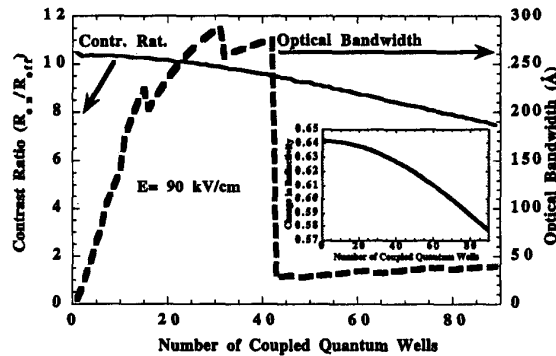
fractive-index changes ( $\Delta n$ ); creating a large chirp coefficient. Here we discuss the experimental creation of asymmetric Fabry-Perot reflection modulators, which incorporate coupled quantum wells in the active region (cavity); yielding pure amplitude reflection modulators with a zero chirp parameter over the entire voltage swing (5 V bias). The asymmetric coupled quantum wells modulate absorption via the spatial separation of carriers [oscillator strength modulation (OSM)] which allows large changes in absorption with zero change in refractive index during switching. Specifically, the coupled-well system used here consists of 50-Å GaAs wells and a 20-Å



CFH6 Fig. 1 Experimental reflectivity versus wavelength for the zero-chirp Fabry-Perot reflection modulator.



CFH6 Fig. 2 Experimental phase versus wavelength for the zero-chirp modulator. Zero-chirp wavelength is 8180 Å. (Inset) Phase versus voltage at the zero-chirp wavelength. (measurement error  $\pm 2^\circ$ ).



CFH6 Fig. 3 Stimulated contrast ratio, optical bandwidth, and change in reflectivity for modulators using coupled quantum wells optimized for maximum change in reflectivity.

$\text{In}_{0.2}\text{Ga}_{0.8}\text{As}$  quantum wells separated by 10-Å  $\text{Al}_{0.33}\text{Ga}_{0.67}\text{As}$  barriers.<sup>1</sup> By using *in situ* growth monitoring, the cavity's Fabry-Perot resonance can be placed at the quantum well zero-chirp wavelength creating reflection modulation. In addition to describing the creation and results of such devices, we describe the limitations on reflectivity changes induced by the use of the OSM technique as compared with other techniques that cannot provide zero chirp.

Experimental results of the total reflectivity versus wavelength are shown in Fig. 1. At 8180 Å, the reflectivity of our device changes from 40% to 70% reflectivity with 5 volts bias. Two techniques were used to extract phase information. First, a direct phase versus voltage measurement was made at 8180 Å using a modified Michelson interferometer setup with an accuracy of around 2°. The inset of Fig. 2 shows reflectivity and phase versus bias at 8180 Å. Phase is unchanging with applied electric field (within our measurement error) until an applied bias of 5.5 V (over the entire voltage range depicted in Fig. 1). Second, because the logarithm of reflected amplitude is related to reflected phase by a Kramers-Kronig relation, a more complete phase picture can be obtained (Fig. 2). Again at 8180 Å, there is no change in reflected phase over the switching cycle.

The main problem with coupled quantum wells is the relatively high value of minimum absorption,  $\alpha_{\text{min}}$ , compared with single-well systems. Limited absorption ratios translate into limited reflectivity changes ( $\Delta R$ ) and contrast ratios. Figure 3 depicts the theoretical design parameter space for coupled quantum well reflection modulators optimized for the maximum change in reflectivity ( $E$  field = 90 kV/cm). The resultant optimization provides  $\Delta R$ s from 57% to 64% and resultant contrast ratios from 8 to 10. Single quantum wells with similar optimization can achieve  $\Delta R > 90\%$ . We discuss further the tradeoffs in device performance required by the use of coupled QWs. In addition, we discuss methods for overcoming performance limitations such as a triple quantum well